Loss of G$_{\alpha 12/13}$ exacerbates apical area dependence of actomyosin contractility

Shicong Xie[a,†], Frank M. Mason[b], and Adam C. Martin[b,*]
[a]Computational and Systems Biology Program and [b]Department of Biology, Massachusetts Institute of Technology, Cambridge, MA 02142

ABSTRACT During development, coordinated cell shape changes alter tissue shape. In the *Drosophila* ventral furrow and other epithelia, apical constriction of hundreds of epithelial cells folds the tissue. Genes in the G$_{\alpha 12/13}$ pathway coordinate collective apical constriction, but the mechanism of coordination is poorly understood. Coupling live-cell imaging with a computational approach to identify contractile events, we discovered that differences in constriction behavior are biased by initial cell shape. Disrupting G$_{\alpha 12/13}$ exacerbates this relationship. Larger apical area is associated with delayed initiation of contractile pulses, lower apical E-cadherin and F-actin levels, and aberrantly mobile Rho-kinase structures. Our results suggest that loss of G$_{\alpha 12/13}$ disrupts apical actin cortex organization and pulse initiation in a size-dependent manner. We propose that G$_{\alpha 12/13}$ robustly organizes the apical cortex despite variation in apical area to ensure the timely initiation of contractile pulses in a tissue with heterogeneity in starting cell shape.

INTRODUCTION

Individual cells often exhibit coordinated shape changes during tissue morphogenesis. Disrupting the coordination of cell shape change can result in defective tissue shapes or ineffectual collective migration (Costa *et al.*, 1994; Weber *et al.*, 2012; Bazellières *et al.*, 2015). Studies have elucidated some mechanisms underlying coordinated cell shape changes or migration, including mechanical feedback between interconnected cells (Fernandez-Gonzalez *et al.*, 2009; Pouille *et al.*, 2009; Cai *et al.*, 2014; Bastounis *et al.*, 2016), extracellular signaling (Wang *et al.*, 2010; Donà *et al.*, 2013), and even response to a global mechanical stress (Aigouy *et al.*, 2010). To achieve coordinated behavior, cells must overcome heterogeneity, including inherent variations in cell shape preceding tissue shape change. Whether there are mechanisms of coordination that overcome heterogeneity in properties such as cell size has, to our knowledge, not been reported.

A model for collective epithelial shape change is the *Drosophila* ventral furrow, where hundreds of cells of the presumptive mesoderm coordinately constrict their apical ends and invaginate into the embryo interior (Figure 1A). In local regions of the ventral furrow, cells constrict with similar rate and timing as their neighbors. However, disrupting a G-protein–coupled receptor (GPCR) pathway, including the secreted ligand Folded gastrulation (Fog) and the G$_{\alpha 12/13}$ protein Concertina (Cta), results in uncoordinated apical constriction (Parks and Wieschaus, 1991; Costa *et al.*, 1994). In *fog* or *cta* mutants, some cells exhibit constriction next to cells that are not constricting or expanding (Sweeton *et al.*, 1991; Oda and Tsukita, 2001). Fog is believed to bind to two or more GPCRs coupled to a heterotrimeric G-protein complex (Kanesaki *et al.*, 2013; Manning *et al.*, 2013; Kerridge *et al.*, 2016). The G$_{\alpha}$ protein, Cta, recruits RhoGEF2 to the apical surface, where it is believed to activate RhoA (Kolsch *et al.*, 2007). RhoA activates the formin Diaphanous (Dia) to stimulate F-actin polymerization, as well as Rho-associated kinase (ROCK) to activate myosin (Figure 1B; Dawes-Hoang *et al.*, 2005; Homem and Peifer, 2009). Previous studies based on apical cell shapes in fixed tissues suggested that a subset of ventral furrow cells stochastically initiate contractility without Cta signaling and use the Cta pathway to up-regulate contractility in neighboring cells and promote collective apical constriction (Sweeton *et al.*, 1991; Costa *et al.*, 1994; Pouille *et al.*, 2009).

Live-imaging studies have revealed that ventral furrow cells constrict in a series of steps, mediated by contractile events called
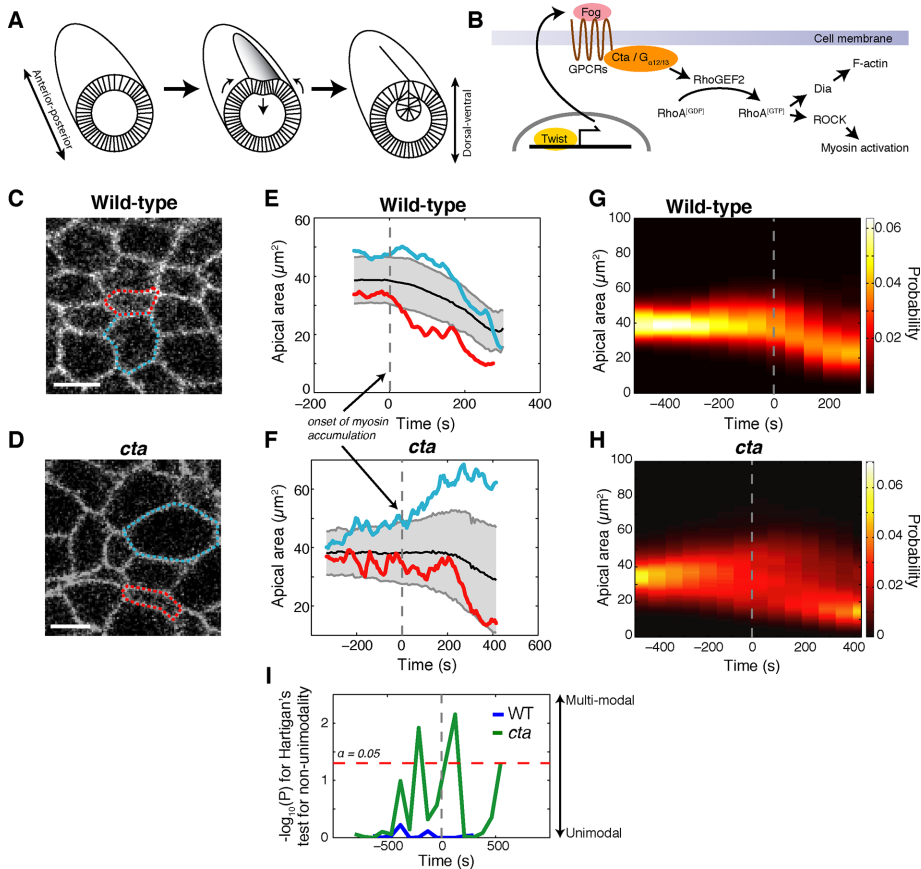
FIGURE 1: Apical area behavior diverges in *cta* cells before actomyosin contractions. (A) Schematic of ventral furrow invagination in the *Drosophila* embryo. (B) Schematic of the Cta pathway. (C, D) Apical cell shape during wild-type (C) and *cta* mutant (D) ventral furrow formation in embryos expressing the membrane marker Gap43::mCherry. Outlined cells are quantified in E and F. (E, F) Cells diverge in constriction behavior in *cta* but not wild-type embryos. Average apical area is shown in black for wild-type (E) and *cta* (F) embryos. Red and cyan traces show individual cell-area time series for the cells highlighted in C and D, respectively. Dashed lines mark the onset of apical myosin accumulation. (G, H) Kernel density estimations of the distribution of apical area as a function of time for wild-type (G) and *cta* (H) embryos. (I) *cta* cells do not apically constrict as a single mode, and area divergence occurs before myosin accumulation. The *p* value for Hartigan's test for nonunimodality shows that *cta* embryos exhibit significant multimodality compared with wild-type embryos (Hartigan and Hartigan, 1985). Red dashed line is $\alpha = 0.05$. Scale bars, 5 µm. Error bars are SDs.

pulses (Martin *et al.*, 2009). Pulses are associated with condensation of both myosin and actin structures (Blanchard *et al.*, 2010; Mason *et al.*, 2013), suggesting that pulses represent transient contractions of an apical actin cortex. The apical domain of a ventral furrow cell is spatially organized, with ROCK being concentrated and stably positioned in the center of the apical cortex (Mason *et al.*, 2013). Because ROCK is concentrated near the apical center and exhibits a radially symmetric decrease in intensity toward the apical margin, we termed this organization radial cell polarity (RCP; Mason *et al.*, 2013). RCP is associated with irreversible or ratcheted contractions by which the contracted cell shape becomes stabilized over time. The transcription factor Twist (Twi) is required for RCP and for cells to transition from having reversible to irreversible contractions (Mason *et al.*, 2013; Xie and Martin, 2015). Twi activates the transcription of *fog* and thus activates the Cta pathway (Figure 1B). It is unclear why loss of either Fog or Cta results in divergent constriction behavior between neighboring cells.

Here we used live imaging of cell shape and a computational framework to identify and classify contractile events to determine how Cta coordinates apical constriction. We found that in the absence of Cta, heterogeneity in nuclear position is associated with variability in the initial apical area before the appearance of apical myosin pulses. Without Cta activity, initially larger apical domains specifically exhibit F-actin and E-cadherin depletion from the apical cortex, and ROCK is not stably centered but drifts back and forth across the apex. We propose that proper organization of the apical cortex leads to the timely initiation of contractile pulses because larger apical area is also associated with a delay in the initiation of contractile pulses, which is preceded by a reduction in apical F-actin. Once cells with larger apical domains start to constrict, they do so normally. Because the constriction timing correlates with starting apical area, we speculate that Cta functions to make cells robust to heterogeneity in apical area, enabling cells with varying areas to initiate contraction in a roughly synchronous manner.

RESULTS

In *cta* mutants, differences in cell shape emerge before apical myosin pulsing

To investigate how Cta coordinates apical constriction in the ventral furrow, we imaged maternal *cta* mutant embryos with fluorescently tagged myosin II regulatory light chain (myosin) and cell membrane (Schüpbach and Wieschaus, 1991; Royou *et al.*, 2002; Martin *et al.*, 2010) and then quantified cell area and apical myosin dynamics. Consistent with previous reports, *cta* cells lack coordinated constriction with neighboring cells, sometimes exhibiting divergent behavior, such as expanding or constricting (Figure 1, C and D; Parks and Wieschaus, 1991; Oda and Tsukita, 2001). Defining the time we first observed apical myosin pulsing in any cell in the embryo as $t = 0$ (Supplemental Figure S1, A–D; see *Materials and Methods*), we found that differences in apical area were present before the appearance of apical myosin pulses and thus before apical contractility has begun (Figure 1, E and F, dashed line, Supplemental Figure S1E, and Supplemental Movie S1). In contrast to wild-type embryos, which apically constrict as a unimodal distribution of apical area over time, *cta* embryos exhibited significant nonunimodality in apical area as they apically constricted (Figure 1, G and H; Xie and Martin, 2015). This revealed an unexpected aspect of the *cta* phenotype, which is that nonunimodality in apical area appeared before the onset of apical myosin pulsing (Figure 1I; Hartigan and Hartigan, 1985). This suggests that a model in which *cta* mutants cause uncoordinated apical constriction by differently regulating apical contractility is not complete because these defects precede myosin pulsing, the known mechanism of apical contractility in these cells (Martin *et al.*, 2009).
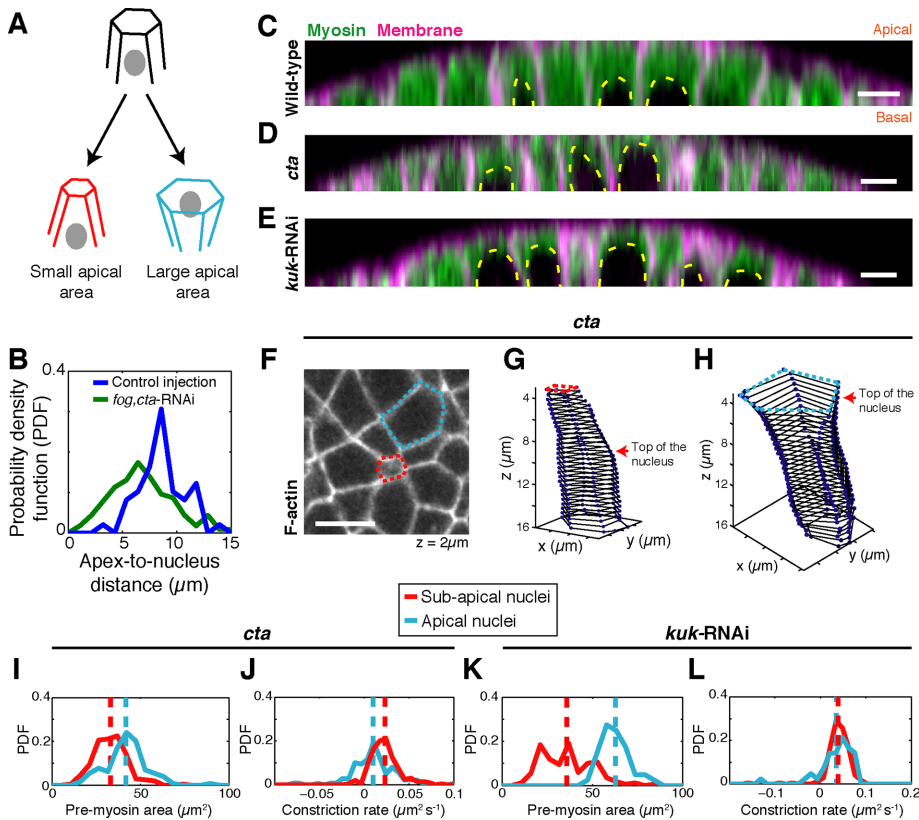
FIGURE 2: Nuclear position alone does not underlie divergent area behavior. (A) Apical-basal nuclear position can bias apical area. (B) The probability density function (PDF) of apex-to-nuclear distance was measured in Histone::GFP *fog,cta*-RNAi cells (*N* = 115) and control-injected cells (*n* = 49; Supplemental Figure S2, A and B). (C–E) Orthogonal views of ventral furrow cells for wild-type (C), *cta* (D), and *kuk*-RNAi (E) embryos expressing Myosin::GFP and membrane marker Gap43::mCherry. Nuclei are visible as dark spots that exclude cytoplasmic myosin signal (yellow outline). (F) Fixed *cta* embryo stained with phalloidin at 2 µm from the apex. Outlined cells are shown in G and H. (G, H) Cells with apical nuclei are apically expanded. Three-dimensional reconstructions of highlighted cells from F are shown with the apical-basal height of the nucleus indicated. (I, K) Apical nuclei are correlated with larger apical area in *cta* and *kuk*-RNAi embryos. The initial apical area is quantified for *cta* (I) and *kuk*-RNAi (K) cells with apical or subapical nuclei. (J, L) Apical nuclei affect apical constriction in *cta* but not *kuk*-RNAi embryos. Constriction rates are quantified for cells with apical or subapical nuclei in *cta* (J) and *kuk*-RNAi (L) embryos. *cta* cells with apical nuclei show significantly lower constriction rate, whereas *kuk*-RNAi cells constrict at similar rates. Scale bars, 5 µm.

cta mutants exhibit aberrant nuclear position and cell shape before constriction

Because our data showed that apical area differences precede apical myosin accumulation, we asked what other properties are heterogeneous in *cta* mutants. We noticed that nuclear apical-basal position is perturbed in *cta* mutant cells (Figure 2A). The top surfaces of nuclei are positioned 6–9 µm from the apical surface in wild-type embryos (Figure 2, B and C). In contrast, we observed that some *cta*-depleted cells had nuclei positioned within 1–2 µm of the apex, as visible by the exclusion of cytoplasmic myosin (Figure 2D) or with green fluorescent protein (GFP)–labeled histone 2A (histone; Figure 2B; $p < 10^{-4}$, one-sided t test; Supplemental Figure S2, A and B). Nuclei in *cta* mutants were apically positioned before observable apical constriction or the onset of apical myosin contractions (Supplemental Figure S2, C and D), suggesting that the increased number of apical nuclei was not simply a result of apical constriction failing to push nuclei basally (Gelbart *et al.*, 2012). We reconstructed cell shapes in fixed *cta* embryos and found that cells with apical nuclei were apically larger but basally smaller, whereas the reverse

was true of cells with basal nuclei (Figure 2, F–H). This suggests that *cta* mutant cells exhibit heterogeneity in cell shape and organization at the onset of contractility, with cells having apical nuclei also having larger apical domains.

To determine whether constriction differences are associated with cells with apical nuclei, we quantified initial apical area as the average cell area 5 min before the onset of myosin accumulation (premyosin apical area). *cta* cells with apical nuclei, defined as cells with nuclei within 5 µm from the apex, exhibited predominantly expanding behavior (Supplemental Figure S2E) and had significantly larger apical area before the onset of myosin pulsing (Figure 2I; $p < 10^{-32}$, Kolmogorov–Smirnov [KS] test). *cta* mutant cells with apical nuclei also constricted more slowly than cells with more subapical nuclei (Figure 2J; $p < 10^{-8}$, KS test). In summary, in *cta* mutants, cells with apically mispositioned nuclei have a larger apical area even before apical myosin pulsing starts in any cell of the embryo, and these cells fail to effectively constrict.

To test whether apical nuclei per se can inhibit apical constriction, we independently perturbed nuclear apical-basal position and quantified the apical area dynamics in the ventral furrow. We injected double-stranded RNA (dsRNA) against *kugelkern* (*kuk*), a known regulator of nuclear morphology and apical-basal position during *Drosophila* cellularization (Brandt *et al.*, 2006; Pilot *et al.*, 2006). Consistent with previous reports, *kuk*–RNA interference (RNAi) embryos had abnormal apically positioned nuclei, similar to *cta* embryos (Figure 2E). In addition, the apical nuclear position introduced significantly more heterogeneity in apical area than for wild-type embryos before the onset of myosin contractility (Supplemental Figure S2F),

with larger apical area being associated with apical nuclei (Figure 2K; $p < 10^{-33}$, one-sided KS test). In contrast to *cta* mutant embryos, which formed sparse apical myosin meshwork that did not span all of the cells, *kuk*-RNAi embryos developed relatively normal ventral furrows, with more continuous myosin distribution (Supplemental Movie S2; Fox and Peifer, 2007). In addition, unlike *cta* mutant embryos, *kuk*-RNAi cells constricted at similar rates regardless of nuclear position (Figure 2L; $p > 0.05$, KS test). Therefore we conclude that the abnormal apical positioning of the nucleus by itself does not impede apical constriction.

Cta is required for the timely initiation of actomyosin pulsing in cells with larger apical area

To understand why cells with apical nuclei and larger apical area in *cta* mutants exhibited reduced constriction rate, we examined different properties of myosin pulses in cells with apical or subapical nuclei. We previously reported that contractile pulses decrease apical area, but are heterogeneous in amplitude, timing, and behavior (whether or not the area decrease is sustained after the pulse; Figure 3A;
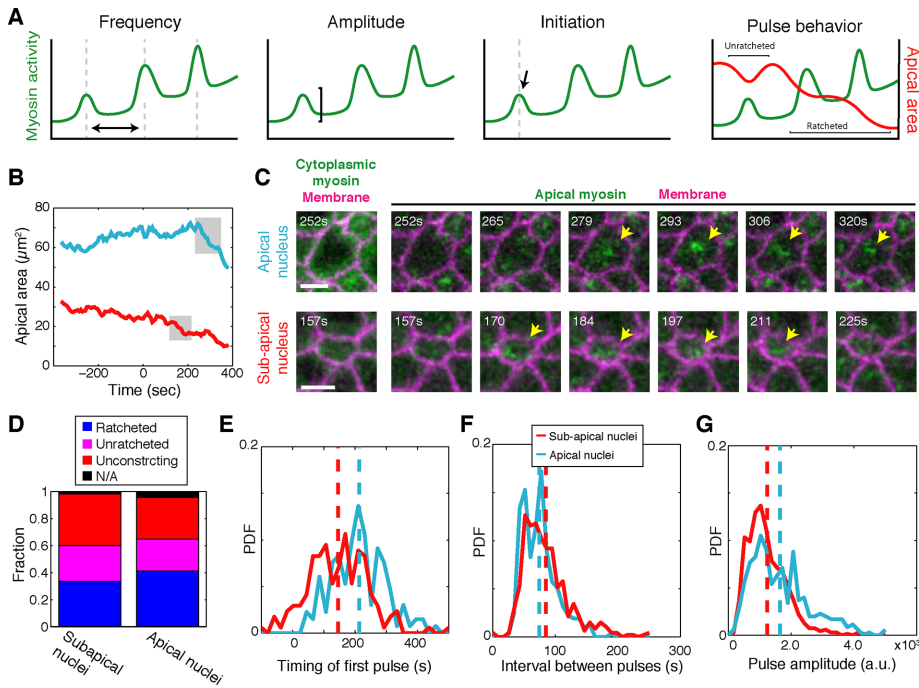
FIGURE 3: Initiation of contraction differentiates constricting and expanding *cta* cells. (A) Schematics of alternative models of different contractile properties associated with constricting or expanding cell area change. (B) Example apical area traces of a *cta* mutant cell with apical nucleus (cyan) and a *cta* mutant cell with a subapical nucleus (red). Pulses shown in C are highlighted in gray. (C) Still images of *cta* mutant cells shown in B from embryos expressing Myosin::GFP and cell membrane marker Gap43::mCherry. Both cells with apical and subapical nuclei exhibit apical myosin pulses (arrows). (D) Distribution of myosin pulse behavior in *cta* mutant cells with apical nuclei vs. subapical nuclei. (E) Expanding cells exhibit delayed contraction initiation compared with constricting cells. The distribution of the first observed myosin pulse is shown for both populations. (F) The distributions of the interval between consecutive pulses are similar for expanding and constricting *cta* cells. (G) Expanding *cta* cells on average exhibit higher pulse amplitude than constricting cells. Scale bars, 5 μm.

In *cta* mutants, cells with large apical area have a defect in apical cortex organization

In ventral furrow cells, the apical cortex is characterized by ROCK, myosin's activator, being localized in the apical center, and junctional proteins, such as E-cadherin, localizing around the circumference (Mason *et al.*, 2013; Vasquez *et al.*, 2014; Xie and Martin, 2015). In embryos depleted of Twist, which functions upstream of Cta, ROCK is mislocalized to junctions (Mason *et al.*, 2013; Xie and Martin, 2015). Therefore we imaged GFP::ROCK and E-cadherin::GFP in *cta* embryos to determine whether their localization was disrupted. In *cta* heterozygotes, ventral furrow cells have ROCK stably positioned in the middle of the apical cortex (Figure 4A, arrowheads). In *cta* homozygous mutant embryos, we found that ROCK organization is different in enlarged cells than in cells that already underwent constriction. Whereas constricted *cta* cells formed a stable, apical ROCK focus (Figure 4B, red arrowheads), ROCK in nonconstricted *cta* mutant cells exhibited aberrant movement, drifting from one side of the apical surface to the other, and also formed multiple apical ROCK patches (Figure 4, B and C, cyan arrows). Because these movements were reminiscent of loss of cell–cell adhesion or cortex–adhesion coupling (Jodoin *et al.*, 2015), we examined how adherens junctions (AJs) are organized in *fog,cta*-RNAi embryos, which phenocopy *cta* mutants. E-cadherin is initially uniform along all cell junctions but is selectively lost or diluted in expanding cell junctions (Figure 4, D and E). Thus loss of Cta disrupts the positioning of ROCK and eventually the stability of E-cadherin specifically in cells that do not immediately undergo constriction.

F-actin can influence AJ stability and affect ROCK localization (Budnar and Yap, 2013; Munjal *et al.*, 2015). To test whether defects in ROCK and E-cadherin localization are associated with an abnormal apical F-actin cortex, we examined homozygous *cta* mutant embryos labeled with Myosin::mCherry and GFP-tagged F-actin–binding domain of utrophin (Utr::GFP; Rauzi *et al.*, 2010). Using subapical F-actin (6 μm below the apex) to segment cell boundaries, we observed that *cta* cells with larger apical area had a more fragmented apical F-actin cortex (Figure 5A, cyan outline). Smaller cells exhibited a more continuous apical cortex (Figure 5A, red outline). To examine how apical area before myosin accumulation relates to F-actin loss, we quantified the apical F-actin density (mean F-actin intensity divided by apical area) within a cell. We found that before the onset of apical myosin accumulation, expanding cells with apical nuclei progressively lost apical F-actin density (Figure 5, B and C). In contrast, smaller *cta* cells with subapical nuclei maintained constant apical F-actin density, similar to wild-type cells (Mason *et al.*, 2013). Of importance, this loss or dilution of apical F-actin from larger *cta* cells with an apical nucleus occurred before the onset of visible myosin pulsing (Figure 5C). Our results suggested that in *cta* mutants, cells that have a larger apical area before the onset of myosin accumulation have a lower

Xie and Martin, 2015). Therefore we compared the timing or quality of myosin pulses between *cta* mutant cells with apical or subapical nuclei.

Similar to wild-type embryos, *cta* mutant embryos exhibited myosin pulses (Figure 3, B and C, and Supplemental Figure S3, A and B), and the area change during a myosin pulse was correlated with myosin intensity (Supplemental Figure S3, C and D). In addition, all three classes of pulses were observed in *cta* mutants independent of nuclear position (Figure 3D and Supplemental Figure S3E). Of interest, we found that cells with apical nuclei had a significant delay in when the first myosin pulse occurred compared with cells with subapical nuclei (Figure 3E and Supplemental Figure S4A; one-tailed KS test, $p < 10^{-7}$). Thus cells that have apical nuclei in *cta* mutants exhibit a delay in initiating contractile pulses and do not constrict well.

Other aspects of pulsing could not explain the expanding behavior of cells with initially large apical areas. It was surprising that cells with apical nuclei had more frequent pulsing, with an average periodicity of 75 s compared with 86 s in smaller cells (Figure 3F and Supplemental Figure S4B; $p < 10^{-3}$, one-sided KS test). Cells with apical nuclei also had higher-intensity pulses (Figure 3G and Supplemental Figure S4C; one-tailed KS test, $p < 10^{-4}$), which we previously showed caused faster apical constriction (Xie and Martin, 2015). Therefore, although myosin pulses were delayed in cells with apical nuclei, pulsing eventually occurred in these cells.

FIGURE 4: Large initial area leads to aberrant RCP in the absence of Cta signaling. (A) Ventral cells display medioapical ROCK foci. Labeled ROCK (GFP::ROCK) and cell membrane (Gap43::mCherry) are shown for *cta*/CyO cells. Arrowheads refer to medioapical ROCK. (B) *cta* mutant cells display heterogeneous radial cell polarity (RCP). ROCK and cell membranes from *cta* mutant embryos expressing GFP::ROCK and Gap43::mCherry are shown for a small *cta* mutant cell next to a larger one. A focus of ROCK forms earlier in the smaller cell (red arrowheads) than in the larger neighboring cell (cyan arrows). Multiple ROCK foci form in the larger cell (arrows). (C) Expanded *cta* mutant cells exhibit ROCK foci that translocate across the apical domain (arrowhead). Shown is a *cta* mutant embryo expressing GFP::ROCK and Gap43::mCherry. (D) AJs are uniformly present in cells from wild-type embryos. Apical E-cadherin and orthogonal views are shown for control-injected embryos expressing E-cadherin::GFP. (E) E-cadherin is depleted from junctions in expanded cells in *fog,cta*-RNAi embryos. Apical E-cadherin and orthogonal views are shown for *fog,cta*-RNAi embryos expressing E-cadherin::GFP. Arrowheads point to cell–cell boundaries that have lost E-cadherin intensity over time. Tick marks show the position of the orthogonal slice. Scale bars, 5 μm.

whether this correlation was detected because of the increased variance in the apical area in *cta* mutants, we also determined this relationship in *kuk-RNAi* embryos, which have greater variance than *cta* mutant embryos but have intact Cta signaling (Supplemental Figures S2F and S5). Although *kuk*-RNAi cells also exhibited a correlation ($R = 0.18$, $p < 0.02$, Spearman's correlation), the relationship was less steep, with a regression coefficient of $1.2 ± 0.8$ s delay per 1 μm^2 of premyosin apical area (Figure 6C and Supplemental Figure S4F). Furthermore, whereas *cta* cells with apical nuclei exhibited significantly delayed initiation of pulsing compared with those with subapical nuclei (Figure 3E), *kuk*-RNAi cells with apical and subapical nuclei initiated pulsing at the same time (Figure 6D; $p > 0.2$, KS-test). Our data reveal that there is a relationship between apical area and timing of the first contractile pulse that is enhanced by Cta (G$_{\alpha12/13}$) loss.

Next we examined the relationship between the premyosin apical area and the density of apical F-actin, defined as the F-actin intensity averaged over the cell apical area. We imaged and compared F-actin levels in *fog,cta*-RNAi and *kuk*-RNAi embryos. Despite an increased heterogeneity in apical area, *kuk*-RNAi cells with larger area did not exhibit lower apical F-actin density (Figure 6E), unlike the *fog,cta*-RNAi cells (Figure 6F). We sorted cells by their premyosin apical area (average area within the first minute) and measured their apical F-actin density over time. *kuk*-RNAi cells starting with larger apical area had F-actin density similar to those with smaller area (Figure 6G). In contrast, initially larger *fog,cta*-RNAi cells had less apical F-actin than smaller ones (Figure 6H). Indeed, initial apical area anticorrelates with time-averaged F-actin density in *cta* mutant cells (Figure 6I; $R = −0.47$, $p < 0.005$, Spearman's correlation) but not *kuk*-RNAi cells ($R = −0.18$, $p > 0.1$). Taken together, our data suggest that Cta is required for a continuous apical F-actin cortex in cells with larger initial apical area, which is associated with timely initiation of contractility.

F-actin density, whereas smaller cells can organize their apical cortex normally.

Loss of Cta enhances the correlation between pulse initiation and initial apical area

To determine the relationship between initiating contractility and apical area, we directly measured this relationship in wild-type and *cta* mutant embryos. In wild-type embryos, there was no correlation between premyosin apical area and the time of the first pulse (Figure 6A and Supplemental Figure S4D; $R = 0.03$, $p > 0.7$, Spearman's correlation). In contrast, *cta* mutant cells' premyosin area was correlated with the timing of the first myosin pulse (Figure 6B and Supplemental Figure S4E; $R = 0.24$, $p < 10^{-4}$), on average being delayed by $2.2 ± 0.9$ s per 1 μm^2 of premyosin apical area. To see

DISCUSSION

Coordinated cellular behavior is seen across tissue development and regeneration, from collective shape changes and collective migration to coordinated cell–cell intercalation (Fernandez-Gonzalez et al., 2009; Friedl and Gilmour, 2009; Tada and Heisenberg, 2012). Furthermore, developing tissues often require cells to behave homogeneously despite inherent heterogeneity in their physical properties. Here we report that Cta allows cells with diverse starting apical areas to initiate contractility at similar times. Because wild-type ventral cells show heterogeneity in their starting apical size (Supplemental Figure S2F), we propose that G$_{\alpha12/13}$ (Cta) promotes
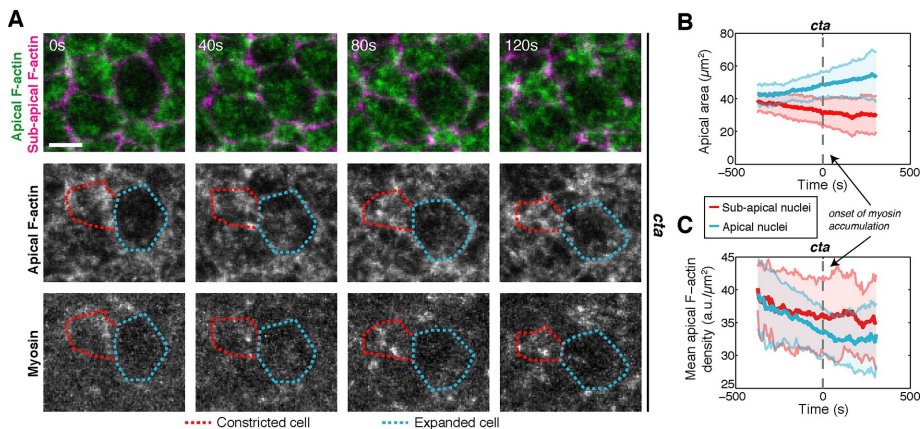
FIGURE 5: Large initial area leads to cortical instability in the absence of Cta signaling. (A) Expanded *cta* cells exhibit defects in apical cortex compared with constricting cells. Maximum intensity projection of the top-4-μm z-slices of Utr::GFP shows the apical F-actin cortex. Utr::GFP at a subapical position (5.6 μm below the apex) shows the cell outlines. The constricted cell exhibits relatively stable apical F-actin, whereas the expanding cell has a less dense apical cortex. (B, C) *cta* cells with apical nuclei cells lose apical F-actin density over time. *cta* cells were grouped according to their nuclear position, and their area dynamics is shown in B. Cells with subapical nuclei maintain constant apical F-actin density, whereas cells with apical nuclei progressively lose apical F-actin (C). Scale bars, 5 μm.

robustness against area-dependent defects in cortex maintenance and contractility. In support of this model, we observe defects in ROCK polarity, AJ localization, and F-actin cortex continuity that exhibit area dependence. These defects are likely to collectively contribute to the delay in actomyosin contraction initiation, which is also correlated with initial apical area. One caveat is that our fluorescent constructs and imaging might not be capturing the true initiation of myosin accumulation. However, our analysis detects low-amplitude myosin pulses that do not reduce apical area, suggesting that we can detect the lower limit of pulses that generate sufficient force to change cell shape (Xie and Martin, 2015). Finally, by comparing the behavior of Cta-depleted cells and *kuk*-RNAi cells with diverse apical area, we show that Cta is needed to robustly initiate contractility and repress apical cortex defects in larger cells.

Previous studies of *fog* mutants suggested that Cta signaling coordinates tissue folding by increasing the number of contracting cells from a few "stochastically" activated cells to a "coherent" activation of contractility across the tissue (Sweeton et al., 1991; Pouille et al., 2009). Our data are consistent with these past studies, in that there are two populations of cells with diverging behavior. However, live imaging and quantitative analysis allowed us to reach a new interpretation for the mechanism of Cta signaling. We find that defects in myosin dynamics and continuity of the apical F-actin meshwork correlate with apical area before apical myosin pulsing and probably underlie the lack of coordinated apical constriction. Cells that initially have smaller apical area are more likely to initiate myosin pulsing early and maintain an intact apical F-actin meshwork; in contrast, cells that start out with larger apical areas tend to display a discontinuous apical F-actin meshwork and subsequent delay in myosin pulsing (Figure 7A). Crucially, tissues with intact Cta signaling but large heterogeneity in initial apical area (i.e., *kuk*-RNAi embryos) do not exhibit as strong a size-dependent defect and constrict in a coordinated manner. This suggests that $G_{\alpha 12/13}$ (Cta) signaling is required in cells to contract over larger apical domain distance. We propose that Cta is required in a length-dependent manner, in which apically larger cells require it to robustly organize their apical domains and initiate contractions in a timely manner (Figure 7B).

An immediate question raised by this study is how Cta ($G_{\alpha 12/13}$) influences the organization of the apical cytoskeleton and AJs to yield robust contractions across larger apical distances. F-actin loss could cause or result from apical expansion; indeed, both defects could reinforce each other. Several features of F-actin meshworks could lead to the area dependence we observe, including actin filament length, number, and cross-linking and the coupling between AJs and the cortex. One possible mechanism is that loss of Cta leads to lower RhoGEF2 activity and therefore RhoA and Dia activity (Kolsch et al., 2007). Dia, a member of the formin family, is both an actin nucleation and elongation factor (Goode and Eck, 2007; Bilancia et al., 2014). Lower Dia activity could sensitize cells that might need more or longer filaments to span a larger apical domain. Alternatively, defects in F-actin seen in *cta* mutant cells could be the direct consequence of disrupting myosin activation by ROCK, because myosin cross-links actin filaments in addition to functioning as a motor. Myosin cross-linking is important for its ability to organize F-actin structures (Ma et al., 2012; Alvarado et al., 2013), and apically larger *cta* cells might require more active myosin for effective cross-linking across larger distances. RhoA is also known to activate LIM kinase to suppress cofilin activity (Maekawa et al., 1999). Actin severing and recycling factors like cofilin are required for stable attachments between the apical cortex and AJs in ventral furrow cells (Jodoin et al., 2015), and also could contribute to the size sensitivity observed in *cta* mutants. Finally, because the actin cortex and AJs cooperate and stabilize each other (Budnar and Yap, 2013; Lecuit and Yap, 2015; Weng and Wieschaus, 2016), a size-dependent defect in actomyosin contractility could fail to stabilize AJs in larger cells, which could feed back on the apical cortex itself. To identify which defect is most upstream, further work is needed to quantify Dia and E-cadherin dynamics in *cta* embryos, as well as uncouple these processes by specific molecular mutations.

One interesting aspect of Cta signaling is its role in positioning the nucleus along the apical-basal axis. We show here that *cta* mutants have a heterogeneous nuclear position, with some cells having abnormal apical nuclei. Although the relatively normal ventral furrow formation of *kuk*-RNAi embryos demonstrates that apical nuclei are not the direct cause of uncoordinated apical constriction, it is nonetheless interesting that Cta affects nuclear position. In the wild-type ventral furrow, the basal migration of nuclei is believed to be a passive response to apical constriction due to volume conservation (Gelbart et al., 2012). In addition, G_α-mediated polar myosin contractions are believed to center the nucleus in the *C. elegans* embryo (Goulding et al., 2007). However, in *cta* cells, the abnormal apical nuclear localization occurs before the onset of apical myosin accumulation, which suggests an alternative mechanism that can position the nuclei. One possible mechanism is centrosomal microtubules, a known mediator of nuclear positioning (Gundersen and Worman, 2013). Alternatively, disrupted actomyosin contractility at the cell's basal or lateral surface before gastrulation could underlie the aberrant nuclear positions. In addition, junctional myosin could be acting to maintain nuclear position or apical size before the onset of apical myosin contractions.
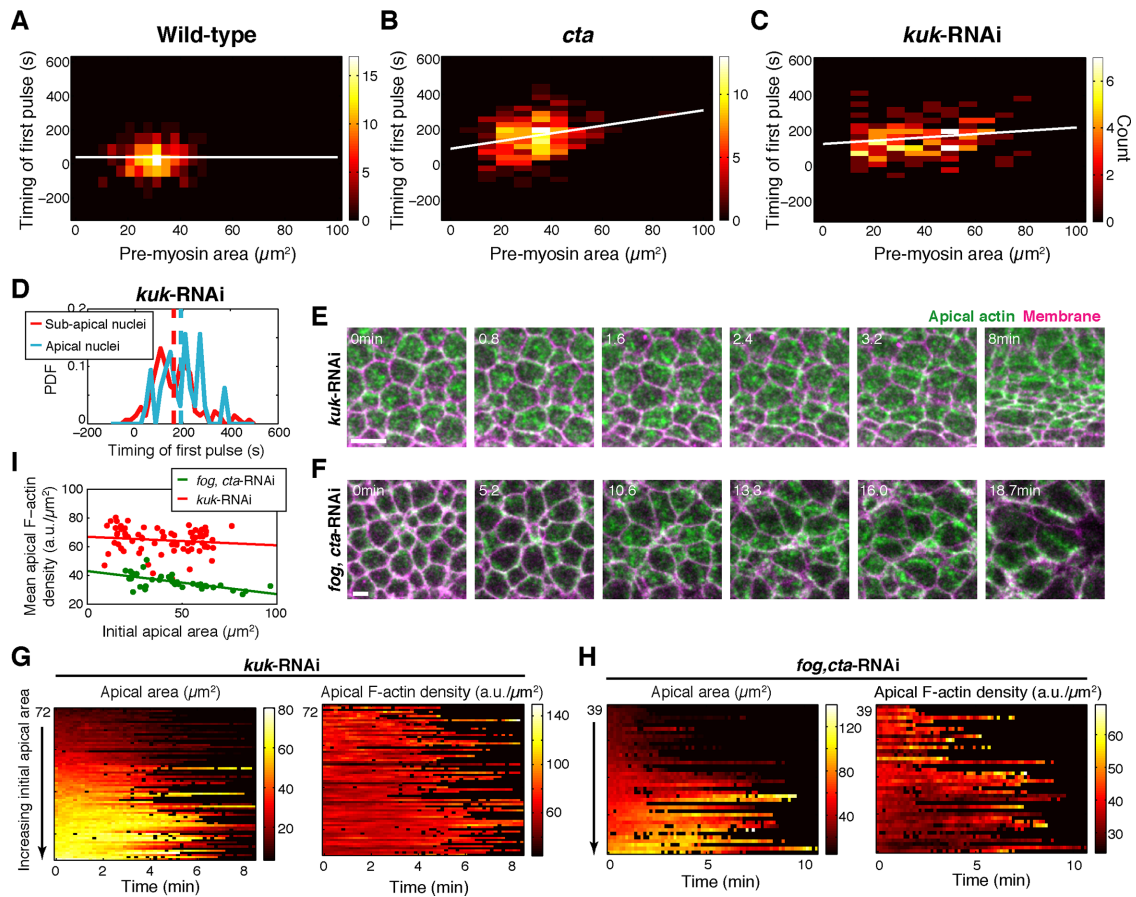
FIGURE 6: Contractility defect is linked to initial apical area in *cta* mutants. (A–C) *cta* cells exhibit higher correlation between premyosin apical area and timing of the first pulse. Histogram of premyosin apical area and the timing of the first pulse for wild-type (A), *cta* mutant (B), and *kuk*-RNAi (C) cells. Line represents best fit. Color bar indicates the count for the number of pulses in each bin. (D) Apical nuclear position does not lead to later pulse initiation in *kuk*-RNAi cells. The timing of the first contraction pulse is quantified for *kuk*-RNAi cells with apical and subapical nuclei. (E, F) F-actin density is lower in initially larger *fog,cta*-RNAi cells but not *kuk*-RNAi cells. Apical F-actin (maximum intensity projection of top-5.2-µm *z*-slices) and cell membrane for *kuk*-RNAi (E) and *fog,cta*-RNAi (F) cells in embryos expressing labeled F-actin, Utr::GFP, and labeled cell membrane, Gap43::mCherry. Scale bars, 5 µm. (G, H) Larger *fog,cta*-RNAi cells have lower F-actin density. The *kuk*-RNAi (G) and *fog,cta*-RNAi (H) cells were sorted by their initial apical area. Sorted apical area and F-actin density time series. Color bar indicates apical area (left) and F-actin density (right). (I) Initial apical area anticorrelates with apical F-actin density (Utr::GFP intensity/area) in *fog,cta*-RNAi cells but not *kuk*-RNAi cells. Initial apical area is quantified against the average apical F-actin density in the first 4 min of ventral furrow formation.

In summary, studies of cell coordination have identified non–cell-autonomous mechanisms of coordination, including cell–cell signaling through chemical or mechanical means (Fernandez-Gonzalez *et al.*, 2009; Donà *et al.*, 2013) or extrinsic signals such as global tissue tension (Aigouy *et al.*, 2010). However, cell-autonomous mechanisms can also coordinate tissue-level behavior by ensuring that cell behaviors are robust against heterogeneity or noise in initial cell properties. Cell geometry has been known to influence acto-myosin organization and activity. The amount of mechanical work done by cells cultured on micropatterened surfaces closely correlates with a cell's spread area (Oakes *et al.*, 2014). Cells also exhibit a characteristic length scale at which they can extend or contract (Vignaud *et al.*, 2012). In the ventral furrow, we propose that Cta signaling buffers the length-dependent sensitivity of the contractile machinery by ensuring the robust organization of apical F-actin and the timely initiation of contractions. Investigation into its molecular mechanism will be crucial for understanding how the contractile machinery functions at different length-scales and how developmental processes might be tuning or shaping their behavior.

MATERIALS AND METHODS

Fly stocks and crosses

The fly stocks used in this study are listed in Table 1. To generate embryos transheterozygous for *cta* with labeled myosin and cell membrane, we crossed *cta^RC10*; *Myosin::GFP, Gap43::mCherry/Tm3* flies with *Df(2L)PR31/CyO, Myosin::GFP* deficiency flies (Schüpbach and Wieschaus, 1989). Nonbalancer F1 were crossed, and F2 embryos were imaged. *cta^RC10* over deficiency F1 females with labeled F-actin or labeled ROCK could not be obtained. Homozygous F-actin–labeled *cta^RC10* embryos were instead obtained by imaging the nonbalancer F1 progeny of cta^RC10/CyO; *Utr::GFP, Sqh::mCherry/Tm3* flies. To obtain homozygous *cta ^RC10* embryos with labeled ROCK and cell membrane, *cta^RC10/CyO; ROCK::GFP* were crossed to *cta^RC10/CyO; Gap43::mCherry/Tm3* flies. Nonbalancer F1 were
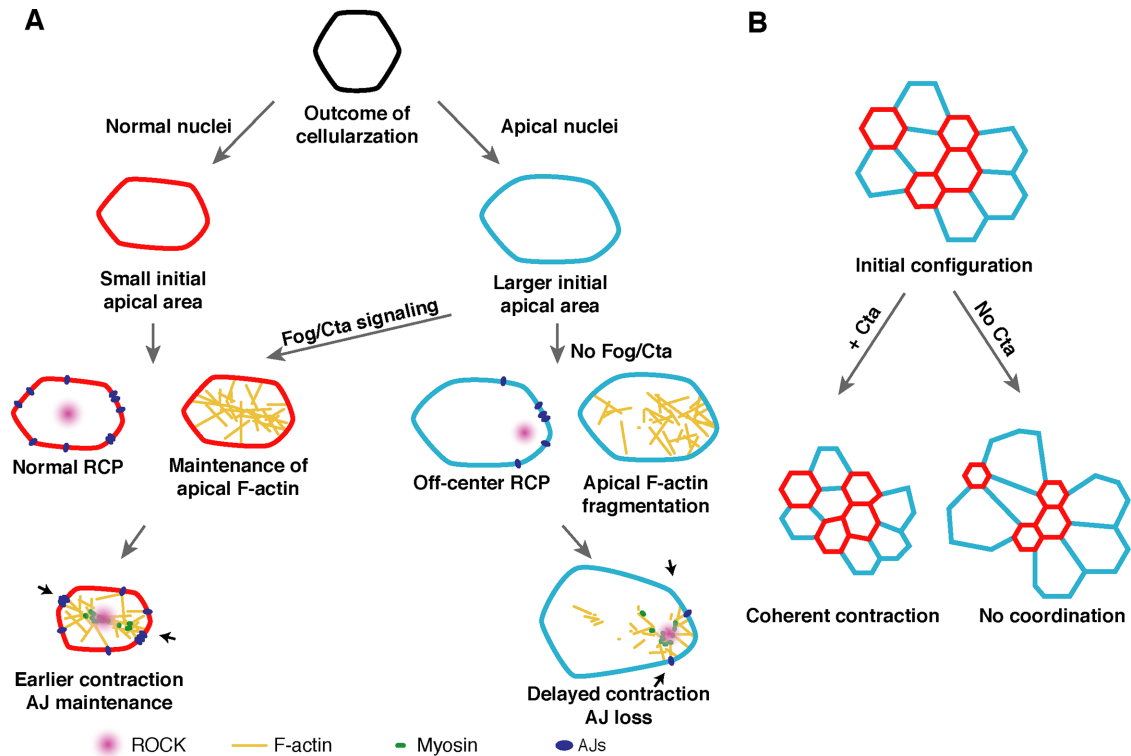
FIGURE 7: Model of Cta-dependent coordination of apical constriction. (A) Loss of Fog/Cta signaling affects apical constriction in a manner modulated by initial apical area. Cells starting with a smaller area establish a ROCK-signaling domain and maintain an apical F-actin network over time. This leads to efficient apical constriction in the cells. In the absence of Fog/Cta, cells starting with a larger area lose apical F-actin and cannot establish a stable ROCK focus. We propose that this leads to delayed contractile pulsing, eventual loss of cell surface E-cadherin, and apical expansion. (B) Model for how the Fog/Cta pathway prevents uncoordinated apical constriction. Red cells are initially smaller. Blue cells are bigger. Fog/Cta enables these cells to constrict together. In contrast, without Fog/Cta, bigger and smaller cells exhibit divergent contractility.

	Stock	Source
1	cta^{RC10}, cn^1, bn^1/CyO	Schüpbach and Wieschaus (1989), gift from E. Wieschaus (Princeton University)
2	Df(2L)PR31/CyO	Gift from E. Wieschaus
3	w; P{w+ sqh^P-GFP::ROCK(K116A)}attP40	Simoes et al. (2010), gift from J. Zallen (Memorial Sloan-Kettering Cancer Center)
4	w; P{w+ sqh^P-UtrABD::GFP}/CyO	Rauzi et al. (2010), gift from T. Lecuit (Institut de Biologie du Développement de Marseille)
5	y, w, sqh^{AX3}, cv; P{w+ sqh^P-Myosin::GFP}42	Royou et al. (2002), Bloomington Drosophila Stock Center (Bloomington, IN)
6	w;; P{w+ sqh^P-Myosin::mCherry}A11	Martin et al. (2009)
7	w;; P{w+ sqh^P-Gap43::mCherry}attP40	Martin et al. (2010)
8	w;; P{w+ ubi^P-H2A::GFP}	Lu et al. (2009), gift from E. Wieschaus
9	w; P{w+ ubi^P-eCadherin::GFP}	Oda and Tsukita (2001), gift from E. Wieschaus
10	cta^{RC10}, cn^1, bn^1/CyO; sqh_P-Myosin::GFP, sqh_P-Gap43::mCherry/Tm3	This study
11	Df(2L)PR31/CyO; P{w+ sqh^P-Myosin::GFP}	Gift from E. Wieschaus
12	cta^{RC10}, cn^1, bn^1/CyO; P{w+ sqh^P-GFP::ROCK(K116A)}attP2	This study
13	cta^{RC10}, cn^1, bn^1/CyO; P{w+ sqh^P-UtrABD::GFP}, P{w+ sqh^P-Myosin::mCherry}A11/Tm3	This study
14	cta^{RC10}, cn^1, bn^1/CyO; P{w+ sqh^P-Gap43::mCherry}attP2/TM3, Sb	This study

TABLE 1: Fly stocks used in this study.

crossed, and F2 embryos were imaged. To generate embryos with labeled myosin and cell membrane for injections, *Myosin::GFP* flies were crossed into *Gap43::mCherry/CyO; Myosin::GFP* flies. Non-balancer F1 were crossed, and F2 embryos were imaged. Embryos with labeled F-actin and cell membrane were generated by crossing *Utr::GFP/CyO* with *Gap43:mCherry/TM3* flies. Nonbalancer F1 were crossed, and F2 embryos were imaged. Embryos with labeled histone and cell membrane were generated by crossing *Histone::GFP* and *Gap::mCherry/CyO* flies. Nonbalancer F1 were crossed, and F2 embryos were imaged.

Immunohistochemstry

For fixed imaging, embryos were dechorionated with bleach and then fixed in a 1:1 mix of 8% paraformaldehyde (PFA) in 0.1 M phosphate buffer, pH 7.4, and 100% heptane for 20–25 min and manually devitellinized. To visualize F-actin after PFA fixation, embryos were incubated with Alexa Fluor 647–phalloidin (Invitrogen, Waltham, MA) in 10% bovine serum albumin (BSA) in phosphate-buffered saline (PBS) plus 0.1% Triton X-100 (PBST) overnight and stained with E-cadherin antibody (DCad-2; Developmental Studies Hybridoma Bank, Iowa City, IA) at 1:50 in 5% BSA in PBST. Embryos were then mounted using AquaPolymount (Polysciences, Warrington, PA).

Imaging

Embryos were dechorionated with 50% commercial bleach and washed with water. They were mounted ventral side up onto a glue-coated slide. Number 1.5 coverslips were glued to either side of the embryo to avoid its compression. A No. 1 coverslip was added on top to create a chamber, into which halocarbon 27 oil was added for imaging. Glue was generated by dissolving double-sided tape in hexane.

Images were acquired on a Zeiss LSM 710 confocal microscope with a 40×/1.2 Apochromat water objective (Zeiss, Oberkochen, Germany). Two-color images were acquired simultaneously. For GFP, a 488-nm argon-ion laser was used for excitation and a 493- to 557-nm bandpass filter for emission. For mCherry, a 561-nm diode laser was used for excitation and a 572- to 700-nm bandpass filter for emission. The pinhole size was set to 2 Airy units.

dsRNA preparation and injection

To generate dsRNA for injection, sequences used against *fog* and *kuk* were as previously reported (Pilot *et al.*, 2006; Martin *et al.*, 2010). *cta* dsRNA sequences were designed with E-RNAi (Arziman *et al.*, 2005). For all sequences, a T7 promoter sequence (5′-TA-ATACGACTCACTATAGGGAGACCAC-3′) was followed by gene-specific sequences: *fog*-F, 5′- TGGTGACCAGTTCTCTTTCC-3′; *fog*-R, 5′-TGTTGCAGTTGCCGAAGT-3′; *cta*-F, 5′-CAGGCCAGACCA-CATAATACC-3′; *cta*-F, 5′-GCGAAACAATACATGAACTCGGC-3′; *kuk*-F, 5′-CAGGCCAGACCACATAATACC-3′; and *kuk*-R, 5′-GCG-AAACAATACATGAACTCGGC-3′.

dsRNA was prepared using the Invitrogen MEGAscript T7 transcription kit and purified using phenol-chloroform RNA extraction and resuspended in 0.1× PBS. For injection, embryos were dechorionated in bleach and desiccated for 4–6 min in anhydrous Drierite. They were mounted ventral side up on a glass slide and covered in injection oil, a 3:1 mixture of halocarbon 800 and halocarbon 27 oils. Borosilicate glass capillary needles were used for injection. To ensure sufficient knockdown of the target gene, all dsRNA injection was done in the blastoderm stage, 2.5–3 h before gastrulation. After injection, the injection oil was removed and replaced with halocarbon 27 oil. The embryos were stored in the dark at room temperature until imaging. Control embryos were injected with 0.1× PBS.

Image processing

All images were filtered with a Gaussian filter of width 1 pixel. To obtain the cell outline, a z-slice of the cell membrane 4–5 µm from the apex was chosen. Apical myosin images were obtained by maximum intensity projection of the apicalmost slices until the chosen membrane slice. Apical myosin images were additionally thresholded using a threshold calculated as 2.5–3.5 SDs above the mean intensity of a subapical, cytoplasmic z-slice in the myosin stack. Subapical cytoplasmic myosin images showing nuclear position were obtained by mean intensity projection of z-slices basal to the chosen membrane slice. Apical F-actin images were obtained by maximum intensity projection of 3- to 4-µm z-slices from the apex. Subapical F-actin images used to identify cell boundaries were chosen at 6–8 µm from the apex.

All image processing was done in FIJI (National Institutes of Health, Bethesda, MD) and MATLAB (MathWorks, Waltham, MA).

Cell segmentation and pulse quantification

Cell segmentation and three-dimensional reconstruction was done with the Embryo Data Geometry Explorer (Gelbart *et al.*, 2012). Pulse quantification was done with a previously published framework, which combines computationally and manually detected myosin pulses to obtain a comprehensive data set of myosin pulsing during ventral furrow formation (Xie and Martin, 2015). We imaged myosin and cell shape in >10 *cta* mutant embryos and chose three representative embryos to perform our segmentation and extensive pulse curation. In *cta* cells, three embryos, 318 cells, and 1127 pulses were analyzed. For *kuk*-RNAi cells, three embryos, 170 cells, and 712 pulses were analyzed. For wild-type cells, 822 pulses from 227 cells in five embryos from the previous study were used. Determination of area behaviors during pulses in *cta* and *kuk*-RNAi cells was done by coclustering them with area response data of pulses from five wild-type and five *twi*-RNAi embryos used in the previous study.

Measuring nuclear position

For *cta* and *kuk*-RNAi embryos with labeled cell membrane and myosin, cells with apical nuclei were identified manually by visualizing each cell in orthogonal view. The nucleus is visualized by the exclusion of cytoplasmic myosin. Cells with nuclei within 0–5 µm of the apex were categorized as having "apical nuclei" and otherwise as having "subapical nuclei."

Apex-to-nucleus distance was determined by visualizing each cell in orthogonal view and measuring the straight-line distance between the vitelline membrane and the top of the nucleus. Still images from Histone-GFP and membrane-mCherry cells were used at the beginning of the movie (*t* = 0 min in Supplemental Figure S2, A and B). Distances were calculated using Fiji/ImageJ.

Embryo temporal alignment

Different ventral furrow movies were aligned by the onset of myosin accumulation. For each movie, 5–10 regions of interest (ROIs) containing the embryo were taken from the maximum intensity projection of the myosin channel. The average myosin intensity was quantified for each ROI as a function of time, and the onset of myosin intensity increase was determined manually from the average intensity curves (Supplemental Figure S1A).

Statistics

For comparing distributions, a two-sided *t* test or KS test was used, as specified in the text. Unless otherwise specified, correlation values are Spearman's correlation, and the *p* value for correlations are against a null hypothesis of no correlation. All statistics were done in MATLAB.

REFERENCES

Aigouy B, Farhadifar R, Staple DB, Sagner A, Röper J-C, Jülicher F, Eaton S (2010). Cell flow reorients the axis of planar polarity in the wing epithelium of Drosophila. Cell 142, 773–786.

Alvarado J, Sheinman M, Sharma A, Mackintosh FC, Koenderink GH (2013). Molecular motors robustly drive active gels to a critically connected state. Nat Phys 9, 591–597.

Arzman Z, Horn T, Boutros M (2005). E-RNAi: a web application to design optimized RNAi constructs. Nucleic Acids Res 33, W582–W588.

Bastounis E, Alvarez-Gonzalez B, del Alamo JC, Lasheras JC, Firtel RA (2016). Cooperative cell motility during tandem locomotion of amoeboid cells. Mol Biol Cell 27, 1262–1271.

Bazellières E, Conte V, Elosegui-Artola A, Serra-Picamal X, Bintanel-Morcillo M, Roca-Cusachs P, Muñoz JJ, Sales-Pardo M, Guimerà R, Trepat X (2015). Control of cell-cell forces and collective cell dynamics by the intercellular adhesome. Nat Cell Biol 17, 409–420.

Bilancia CG, Winkelman JD, Tsygankov D, Nowotarski SH, Sees JA, Comber K, Evans I, Lakhani V, Wood W, Elston TC, et al. (2014). Enabled negatively regulates diaphanous-driven actin dynamics in vitro and in vivo. Dev Cell 28, 394–408.

Blanchard GB, Murugesu S, Adams RJ, Martinez-Arias A, Gorfinkiel N (2010). Cytoskeletal dynamics and supracellular organisation of cell shape fluctuations during dorsal closure. Development 137, 2743–2752.

Brandt A, Papagiannouli F, Wagner N, Wilsch-Bräuninger M, Braun M, Furlong EE, Loserth S, Wenzl C, Pilot F, Vogt N, et al. (2006). Developmental control of nuclear size and shape by Kugelkern and Kurzkern. Curr Biol 16, 543–552.

Budnar S, Yap AS (2013). A mechanobiological perspective on cadherins and the actin-myosin cytoskeleton. F1000Prime Rep 5, 35.

Cai D, Chen S-C, Prasad M, He L, Wang X, Choesmel-Cadamuro V, Sawyer JK, Danuser G, Montell DJ (2014). Mechanical feedback through E-cadherin promotes direction sensing during collective cell migration. Cell 157, 1146–1159.

Costa M, Wilson ET, Wieschaus E (1994). A putative cell signal encoded by the folded gastrulation gene coordinates cell shape changes during Drosophila gastrulation. Cell 76, 1075–1089.

Dawes-Hoang RE, Parmar KM, Christiansen AE, Phelps CB, Brand AH, Wieschaus EF (2005). folded gastrulation, cell shape change and the control of myosin localization. Development 132, 4165–4178.

Donà E, Barry JD, Valentin G, Quirin C, Khmelinskii A, Kunze A, Durdu S, Newton LR, Fernandez-Minan A, Huber W, et al. (2013). Directional tissue migration through a self-generated chemokine gradient. Nature 503, 285–289.

Fernandez-Gonzalez R, Simoes S de M, Röper J-C, Eaton S, Zallen JA (2009). Myosin II dynamics are regulated by tension in intercalating cells. Dev Cell 17, 736–743.

Fox DT, Peifer M (2007). Abelson kinase (Abl) and RhoGEF2 regulate actin organization during cell constriction in Drosophila. Development 134, 567–578.

Friedl P, Gilmour D (2009). Collective cell migration in morphogenesis, regeneration and cancer. Nat Rev Mol Cell Biol 10, 445–457.

Gelbart MA, He B, Martin AC, Thiberge SY, Wieschaus EF, Kaschube M (2012). Volume conservation principle involved in cell lengthening and nucleus movement during tissue morphogenesis. Proc Natl Acad Sci USA 109, 19298–19303.

Goode BL, Eck MJ (2007). Mechanism and function of formins in the control of actin assembly. Annu Rev Biochem 76, 593–627.

Goulding MB, Canman JC, Senning EN, Marcus AH, Bowerman B (2007). Control of nuclear centration in the C. elegans zygote by receptor-independent Galpha signaling and myosin II. J Cell Biol 178, 1177–1191.

Gundersen GG, Worman HJ (2013). Nuclear positioning. Cell 152, 1376–1389.

Hartigan JA, Hartigan PM (1985). The dip test of unimodality. Ann Statist 13, 70–84.

Homem CCF, Peifer M (2009). Exploring the roles of diaphanous and enabled activity in shaping the balance between filopodia and lamellipodia. Mol Biol Cell 20, 5138–5155.

Jodoin JN, Coravos JS, Chanet S, Vasquez CG, Tworoger M, Kingston ER, Perkins LA, Perrimon N, Martin AC (2015). Stable force balance between epithelial cells arises from F-actin turnover. Dev Cell 35, 685–697.

Kanesaki T, Hirose S, Grosshans J, Fuse N (2013). Heterotrimeric G protein signaling governs the cortical stability during apical constriction in Drosophila gastrulation. Mech Dev 130, 132–142.

Kerridge S, Munjal A, Philippe J-M, Jha A, Las Bayonas de AG, Saurin AJ, Lecuit T (2016). Modular activation of Rho1 by GPCR signalling imparts polarized myosin II activation during morphogenesis. Nat Cell Biol 18, 261–270.

Kolsch V, Seher T, Fernandez-Ballester GJ, Serrano L, Leptin M (2007). Control of Drosophila gastrulation by apical localization of adherens junctions and RhoGEF2. Science 315, 384–386.

Lecuit T, Yap AS (2015). E-cadherin junctions as active mechanical integrators in tissue dynamics. Nat Cell Biol 17, 533–539.

Lu X, Li JM, Elemento O, Tavazoie S, Wieschaus EF (2009). Coupling of zygotic transcription to mitotic control at the Drosophila mid-blastula transition. Development 136, 2101–2110.

Ma X, Kovács M, Conti MA, Wang A, Zhang Y, Sellers JR, Adelstein RS (2012). Nonmuscle myosin II exerts tension but does not translocate actin in vertebrate cytokinesis. Proc Natl Acad Sci USA 109, 4509–4514.

Maekawa M, Ishizaki T, Boku S, Watanabe N, Fujita A, Iwamatsu A, Obinata T, Ohashi K, Mizuno K, Narumiya S (1999). Signaling from Rho to the actin cytoskeleton through protein kinases ROCK and LIM-kinase. Science 285, 895–898.

Manning AJ, Peters KA, Peifer M, Rogers SL (2013). Regulation of epithelial morphogenesis by the G protein-coupled receptor mist and its ligand fog. Sci Signal 6, ra98.

Martin AC, Gelbart M, Fernandez-Gonzalez R, Kaschube M, Wieschaus EF (2010). Integration of contractile forces during tissue invagination. J Cell Biol 188, 735–749.

Martin AC, Kaschube M, Wieschaus EF (2009). Pulsed contractions of an actin-myosin network drive apical constriction. Nature 457, 495–499.

Mason FM, Tworoger M, Martin AC (2013). Apical domain polarization localizes actin-myosin activity to drive ratchet-like apical constriction. Nat Cell Biol 15, 926–936.

Munjal A, Philippe J-M, Munro E, Lecuit T (2015). A self-organized biomechanical network drives shape changes during tissue morphogenesis. Nature 524, 351–355.

Oakes PW, Banerjee S, Marchetti MC, Gardel ML (2014). Geometry regulates traction stresses in adherent cells. Biophys J 107, 825–833.

Oda H, Tsukita S (2001). Real-time imaging of cell-cell adherens junctions reveals that Drosophila mesoderm invagination begins with two phases of apical constriction of cells. J Cell Sci 114, 493–501.

Parks S, Wieschaus E (1991). The Drosophila gastrulation gene concertina encodes a G alpha-like protein. Cell 64, 447–458.

Pilot F, Philippe J-M, Lemmers C, Chauvin J-P, Lecuit T (2006). Developmental control of nuclear morphogenesis and anchoring by charleston, identified in a functional genomic screen of Drosophila cellularisation. Development 133, 711–723.

Pouille P-A, Ahmadi P, Brunet A-C, Farge E (2009). Mechanical signals trigger Myosin II redistribution and mesoderm invagination in Drosophila embryos. Sci Signal 2, ra16.

Rauzi M, Lenne P-F, Lecuit T (2010). Planar polarized actomyosin contractile flows control epithelial junction remodelling. Nature 468, 1110–1114.

Royou A, Sullivan W, Karess R (2002). Cortical recruitment of nonmuscle myosin II in early syncytial Drosophila embryos: its role in nuclear axial expansion and its regulation by Cdc2 activity. J Cell Biol 158, 127–137.

Schüpbach T, Wieschaus E (1989). Female sterile mutations on the second chromosome of Drosophila melanogaster. I. Maternal effect mutations. Genetics 121, 101–117.

Schüpbach T, Wieschaus E (1991). Female sterile mutations on the second chromosome of Drosophila melanogaster. II. Mutations blocking oogenesis or altering egg morphology. Genetics 129, 1119–1136.

Simoes S de M, Blankenship JT, Weitz O, Farrell DL, Tamada M, Fernandez-Gonzalez R, Zallen JA (2010). Rho-kinase directs Bazooka/Par-3 planar polarity during Drosophila axis elongation. Dev Cell 19, 377–388.

Sweeton D, Parks S, Costa M, Wieschaus E (1991). Gastrulation in Drosophila: the formation of the ventral furrow and posterior midgut invaginations. Development 112, 775–789.

Tada M, Heisenberg CP (2012). Convergent extension: using collective cell migration and cell intercalation to shape embryos. Development 139, 3897–3904.

Vasquez CG, Tworoger M, Martin AC (2014). Dynamic myosin phosphorylation regulates contractile pulses and tissue integrity during epithelial morphogenesis. J Cell Biol 206, 435–450.

Vignaud T, Galland R, Tseng Q, Blanchoin L, Colombelli J, Théry M (2012). Reprogramming cell shape with laser nano-patterning. J Cell Sci 125, 2134–2140.

Wang X, He L, Wu YI, Hahn KM, Montell DJ (2010). Light-mediated activation reveals a key role for Rac in collective guidance of cell movement in vivo. Nat Cell Biol 12, 591–597.

Weber GF, Bjerke MA, DeSimone DW (2012). A mechanoresponsive cadherin-keratin complex directs polarized protrusive behavior and collective cell migration. Dev Cell 22, 104–115.

Weng M, Wieschaus E (2016). Myosin-dependent remodeling of adherens junctions protects junctions from Snail-dependent disassembly. J Cell Biol 212, 219–229.

Xie S, Martin AC (2015). Intracellular signalling and intercellular coupling coordinate heterogeneous contractile events to facilitate tissue folding. Nat Commun 6, 7161.